29 August 2025
matteo.paul.giacomelli@cern.ch

Slow Extraction with Crystal from the SPS

Matteo Paul Giacomelli, Yann Dutheil, Aleksandr Gorn
CERN, CH-1211 Geneva, Switzerland

Keywords: SPS, Slow Extraction, Crystal Channeling, Xsuite

Summary

The third-integer resonant extraction (3rd IRE) of the proton beam from the Super Proton Synchrotron (SPS) is a critical technique used for slow extraction of particles, enabling precise delivery of protons for various high-energy physics experiments. In this method, the beam is driven into a controlled resonance condition where the horizontal oscillation frequency of the protons becomes a rational fraction (one third) of the machine's natural frequency. This resonance, enhanced by sextupole magnets, excites stable particles beyond the separatrix and gradually extracts them over a period of time, allowing for a continuous and tunable beam spill.

However, a significant challenge of this technique is the radio-activation of key components, particularly the ZS (Z-septum) device. The ZS, which is responsible for deflecting the extracted particles, experiences intense proton interactions, leading to significant activation over time. This radio-activation complicates maintenance procedures, increases radiation exposure risks to personnel, and requires frequent interventions for decontamination.

To address this issue, an active research and development effort is aimed at replacing the ZS with bent crystals. Bent crystals have the potential to guide the beam particles with higher precision and lower interaction rates, significantly reducing the levels of radio-activation. The crystal channelling technique leverages the electromagnetic potential within a bent crystal lattice to coherently deflect particles along specific trajectories. This innovative approach promises not only to mitigate the activation problem but also to enhance the overall efficiency and control of the slow extraction process. The adoption of bent crystals could lead to safer, more reliable, and cost-effective operations within the SPS accelerator complex.

In conclusion, while third-integer resonant extraction remains a cornerstone of proton beam manipulation in high-energy physics, the transition to bent crystal technologies holds the potential to revolutionize the method, addressing the long-standing issue of radio-activation and improving long-term operational sustainability.

Contents

1 Introduction

The Super Proton Synchrotron (SPS) at CERN is a circular accelerator with a circumference of 6.9 km that serves both as an injector to the Large Hadron Collider (LHC) and as a provider of high-intensity beams for fixed-target experiments. One of its main extraction lines, TT20, delivers protons from the SPS to the North Area experimental halls as it is shown in Fig. 1. This facility hosts a wide range of physics programs, from hadron structure studies to searches for rare processes, making it one of the most versatile experimental areas at CERN.

The SHiP (Search for Hidden Particles) experiment is a proposed fixed-target facility at the CERN SPS aiming to investigate physics beyond the Standard Model. The experiment will make use of the high-intensity 400 GeV proton beam slowly extracted from the SPS and directed onto a heavy target, producing a large flux of secondary particles. In addition to its physics programme, SHiP has also motivated investigations into novel beam extraction and collimation schemes using bent crystals. These studies explore the possibility of exploiting crystal channelling and volume reflection to deflect or extract protons with high efficiency, providing an attractive alternative [1] to conventional slow-extraction techniques. Such crystal-based concepts are of particular interest in the high-intensity environment foreseen for SHiP, where minimizing beam losses and activation is essential.

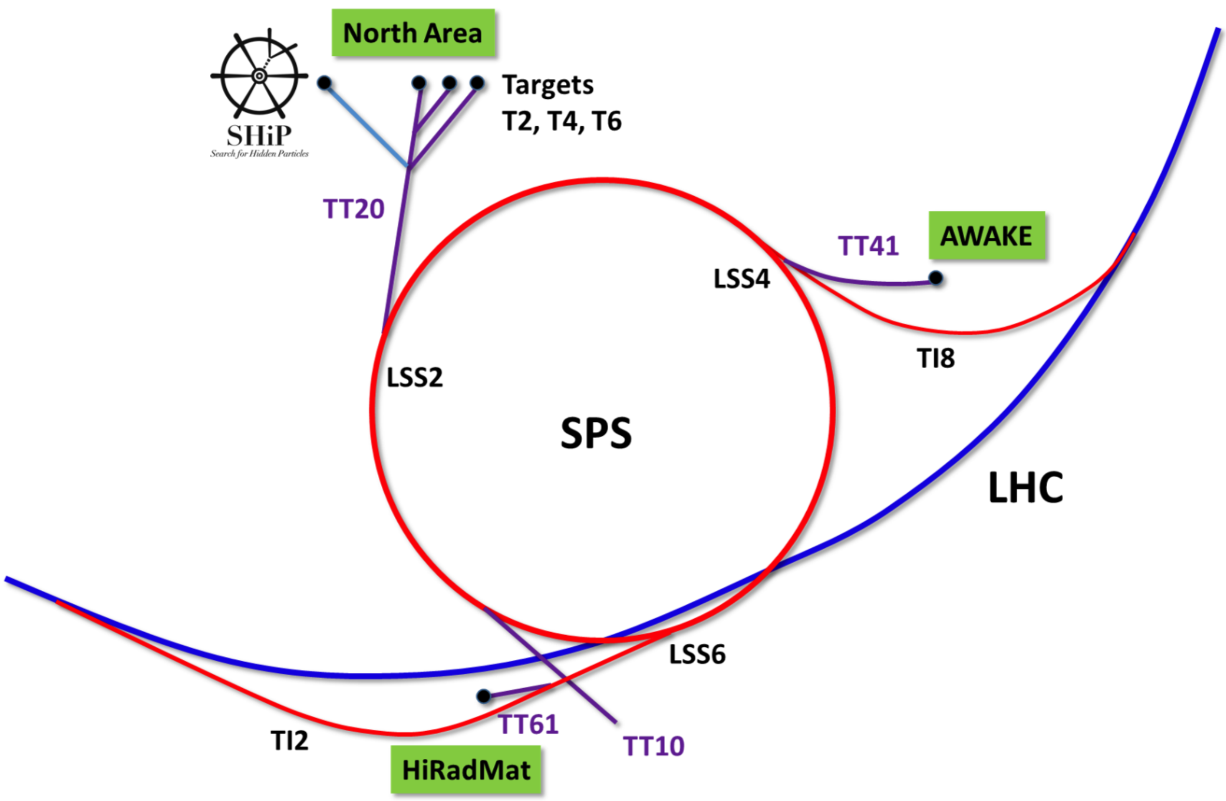

Figure 1: Schematic of the SPS made by the SHiP collaboration [2].

The TT20 is the transfer line that brings the proton beam from the SPS to the North Area (NA) where the fixed target experiments are located. The extraction into TT20 is realized through a sequence of septa [3] in Long Straight Section 2 (LSS2).

The first element encountered in LSS2 is the electrostatic septum (ZS), consisting of a plane of ultra-thin tungsten wires placed in a high-voltage electrostatic field. The ZS provides the initial deflection, on the order of tens of micro-radians, which separates the extracted slice of the beam from the circulating beam. Because of the unavoidable particle interactions with the septum wires, the ZS is the dominant source of beam losses and local activation during extraction. Downstream of the ZS, the TPST collimator (this collimator is 4.2 mm thick and located on the outer side of the ring) is installed to intercept mis-steered particles and protect the subsequent septa from direct impacts. The extraction angle is then amplified by a series of magnetic septa, namely the MSE and MST, which provide strong dipole fields while maintaining a field-free channel for the circulating beam. These magnets deliver the bulk of the horizontal deflection required to cleanly transfer the extracted beam into the TT20 line, where it is transported toward the North Area fixed-target experimental facilities.

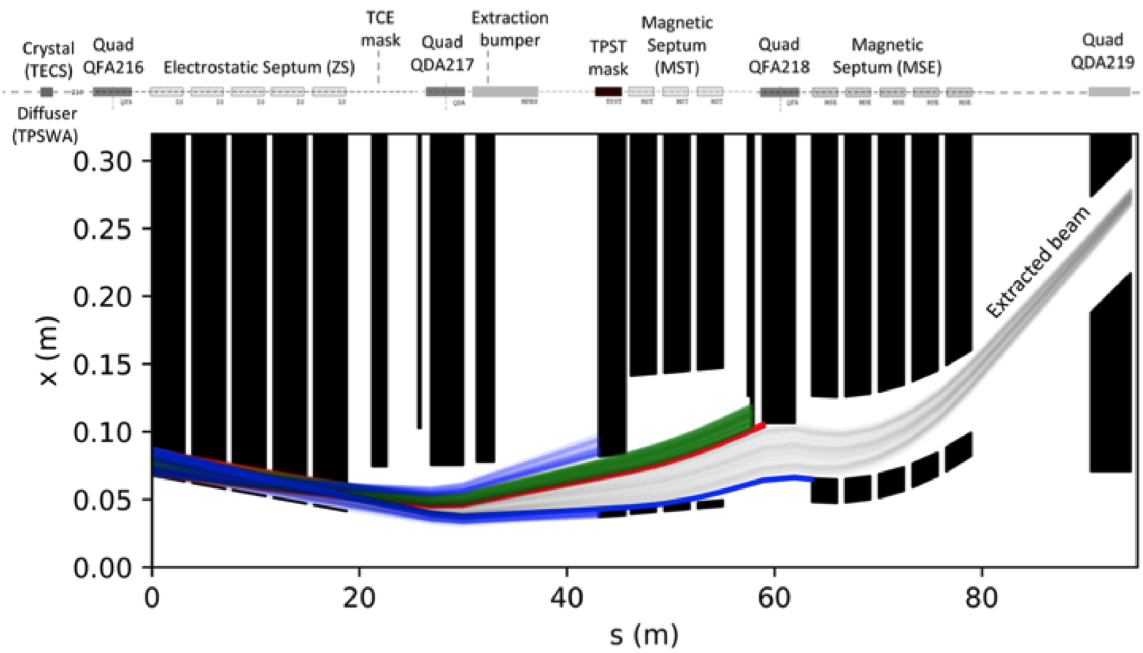

Figure 2: Schematic of the LSS2 extraction line [4].

In parallel to the conventional septa, two bent silicon crystals are installed in the SPS to investigate crystal-assisted extraction schemes. The **TECA** crystal, located in LSS4, is employed for non-local shadowing [5]. Conversely, the **TECS** crystal, positioned in LSS2 just upstream of the electrostatic septum, acts as a local shadowing device [6]. It channels particles that would otherwise intercept the septum wires, thereby reducing losses and radio-activation at the ZS. Together, TECA and TECS provide complementary approaches to loss mitigation and form an essential testbed for the development of crystal-assisted slow extraction in the SPS.

1.1 ZS septum

The electrostatic septum (ZS) is the first element of the SPS slow extraction system as it is shown in Fig. 3. The ZS is divided into 5 separate tanks, 3.1 m in length, each containing an array of 2080 W-Re wires that create the boundary delimiting the low and high electric field regions. The wires are made as thin as possible (ZS 1-2: 60 µm diameter, ZS 3-5: 100 µm diameter) in order to reduce beam losses, but a small fraction of beam is unavoidably scattered on the wires, inducing radioactivity in LSS2.

A fundamental limitation of the ZS is that a significant fraction of the extracted beam inevitably intercepts the septum wires. At SPS energies (400 GeV), even a small impact rate translates into considerable power deposition in the wires, causing increased temperature, mechanical stress, and enhanced secondary particle production. These secondary showers lead to substantial *radio-activation* of the ZS region, which in turn restricts access for maintenance and poses a challenge for high-intensity operation [7]. Mitigation strategies, such as optimised orbit bumps, collimator shadowing, or crystal-assisted extraction, are actively studied to reduce the beam fraction lost on the ZS wires.

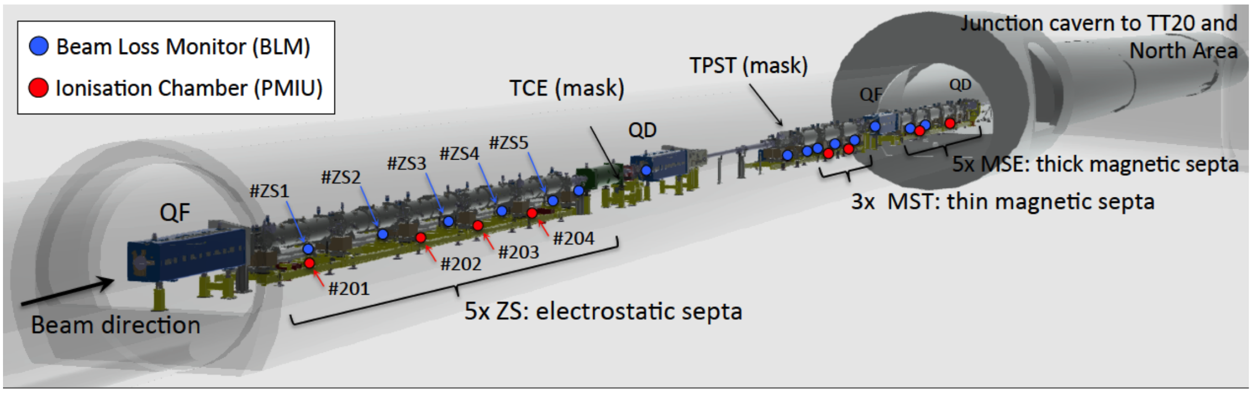

Figure 3: 3D schematic of the LSS2 extraction region [8].

1.2 Slow extraction in the SPS

Slow extraction is the process of extracting a fraction of the circulating beam from the SPS over several seconds, in order to provide a continuous and quasi-uniform spill to the fixed-target experiments in the North Area. This approach enables a controlled delivery of protons to the experimental facilities, in contrast to fast single-turn extraction which would deliver the full beam intensity in one pulse. Slow resonant extraction in the SPS at CERN has undergone continuous optimization over several decades [9]. A key challenge remains the minimization of beam losses [10], which is essential to preserve the integrity of accelerator components and limit radiation exposure to personnel.

1.2.1 Third-Integer Slow Resonant Extraction

The standard slow extraction mode at the SPS exploits the third-integer resonance of the horizontal betatron tune. By adjusting the machine tune close to $Q_x = n/3$, with n an integer, a triangular separatrix is formed in phase space as shown in Fig. 4. As the tune is driven closer to the resonance, particles diffuse across the separatrix and are progressively extracted from the stable area. This controlled diffusion ensures that particles approach the ZS over many turns, where a small fraction of the beam is deflected and subsequently transported by the downstream magnetic septa into TT20. The method allows the extraction of up to several seconds long spills, which are required by the fixed-target experiments in the North Area. However, the unavoidable interception of particles on the thin ZS wires remains the main source of beam loss and activation during this process.

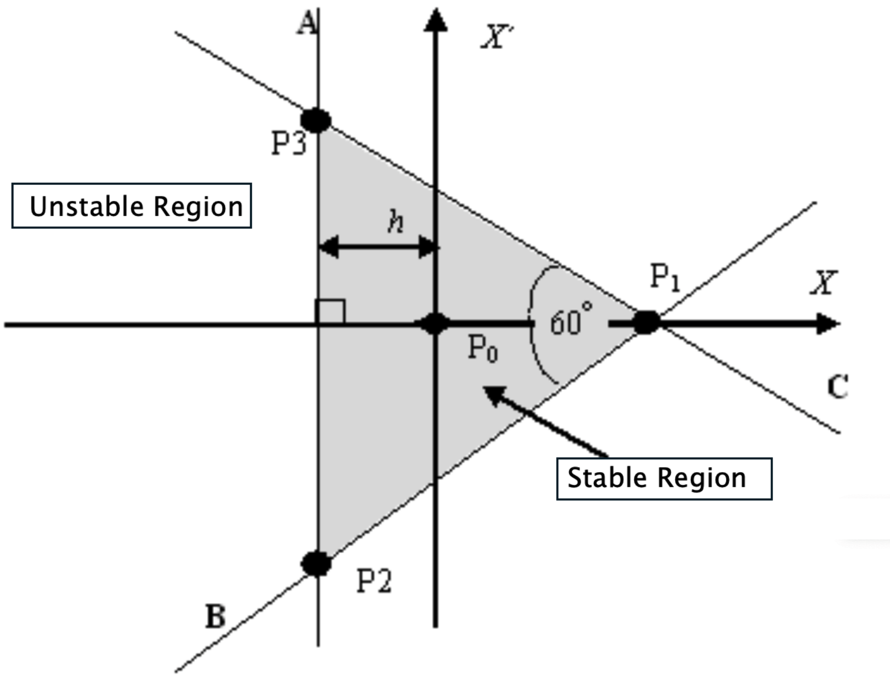

Figure 4: 3rd Integer Slow extraction phase space [11].

1.2.2 Non-resonant Slow extraction with crystal

In this chapter is explained a new scheme for slow extraction without the use of the ZS. Instead, it's the TECA crystal to provide the initial kick to the particles getting extracted. This new scheme for slow extraction is non-resonant because doesn't use the third integer excitation of the horizontal tune. The crystal channelling simulations and the design of the new optics for the non-resonant slow extraction scheme were bench-marked with Xsuite [12] framework tailored for high fidelity modeling of the beam dynamics in particle accelerators.

This novel non-resonant slow extraction scheme [13] is being investigated to reduce radio-activation of the electrostatic septum. The TPST in the extraction line is protecting the first downstream thin MST. After removing the ZS from the extraction line, the TPST becomes the first element to interact with the beam instead of the fragile blades of the electrostatic septum.

Of the different extraction schemes considered for slow extraction from the SPS, the approach investigated in these studies is based on driving the beam into the crystal using **dispersion** as shown in Fig. 5, by creating a controlled orbit bump that shifts the beam horizontally as a function of momentum deviation, allowing particles with increasing momentum to gradually be extracted via interaction with the crystal. The objective is to generate a beam with a large normalised horizontal dispersion at the TECA location in order to slowly push the beam into the crystal acceptance via change of the reference momentum p_0 similarly to Constant Optics Slow Extraction (COSE) [14].

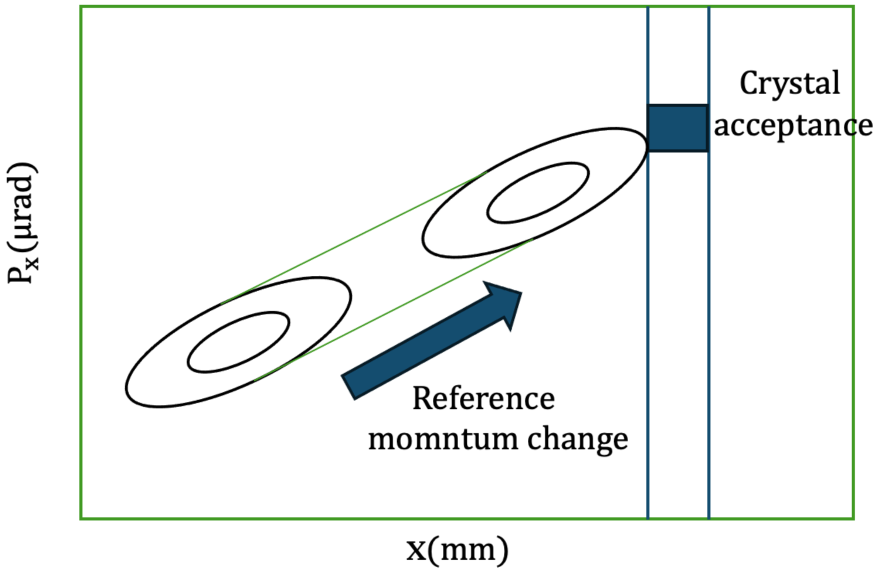

Figure 5: Schematic representation of the phase space of the dispersion-driven steering to the crystal.

The beam size

$$\sigma_x = \sqrt{\beta_x \varepsilon_x + D_x^2(\delta p/p_0)^2}, \tag{1}$$

must be dominated by dispersion, enabling precise control over beam steering into the crystal. A large dispersion at the crystal position allows the beam to be gradually steered towards the crystal's acceptance via reference momentum change. The total relative momentum spread $\delta p/p_0$ used for the studies was 1.5×10^{-3}.

To quantify the response to the kick received by the channelled beam the transfer matrix is calculated from TECA to the TPST collimator and estimate the beam position at this element: $x_{col} = R_{11} x_{\mathrm{cry}} + R_{12} x'_{\mathrm{cry}}$. The separation between the channelled and non-channelled particles is given by

$$\Delta x_{col} = \sqrt{\beta_{cry}\beta_{\mathrm{col}}}\,\sin(\Delta\phi) \cdot \Delta x'_{cry} \tag{2}$$

where $\Delta x'_{cry}$ is the bending angle of crystal. This separation is maximized when the betatron phase advance between the crystal and each collimator satisfies $\Delta\phi = \pi/2 + \pi n$, where n is any integer number.

2 Bent crystals for accelerators

Bent crystals are used in particle accelerators to coherently steer charged particles through the phenomenon of channelling [15], where particles are guided by the electrostatic potential between crystal planes. By precisely bending the crystal as shown in Fig. 6, the lattice planes act like a set of microscopic "rails", deflecting the particles by µrads over just a few millimeters of material. This technique is exploited for beam collimation, extraction, and halo cleaning [16], as it allows highly efficient deflection with minimal material interaction compared to conventional magnets, thus reducing losses and radiation in sensitive areas.

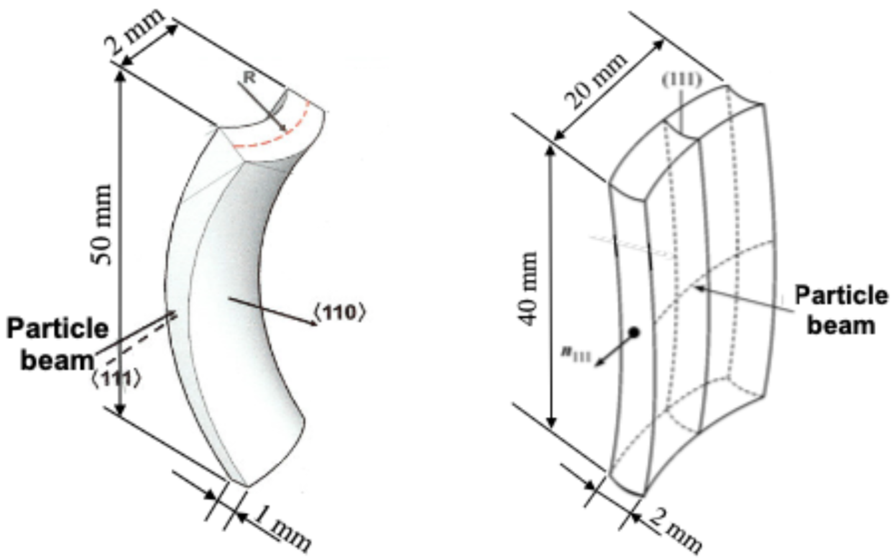

Figure 6: Geometrical bending of a strip (left) and a quasi-mosaic (right) crystal, together with typical dimensions of crystals used in the SPS.

There are four main scenarios that can happen when a particle interacts with a bent silicon crystal: channelling (**CH**), volume reflection (**VR**), de-channelling (**DC**), volume capture(**VC**) and amorphous scattering (**AM**). Depending on the impacting angle of the particles respect to the crystal, the scenarios have different probabilities of happening as it is possible to see in Fig. 7. When a charged particle enters a crystal with an angle smaller than the critical angle θ_c, it is captured between atomic planes, experiencing a continuous potential well. The critical angle is:

$$\theta_c = \sqrt{\frac{2U_0}{E}}$$

where U_0 (25 eV for silicon) is the planar potential depth and E is the particle's energy. From this relation, it follows that the critical angle decreases with increasing particle energy as it is possible to observe in Tab. 1. In practice, this means that higher-energy particles require a more precise alignment with the crystal planes in order to be efficiently channeled, while lower-energy particles can enter the channelling regime under a wider angular acceptance.

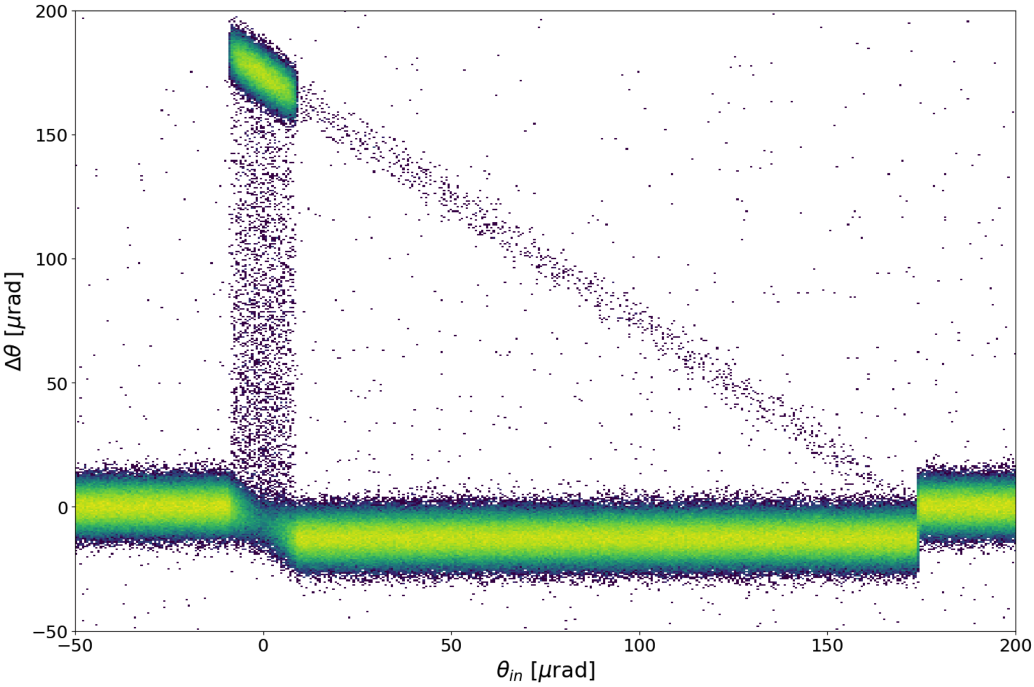

Figure 7: Angle vs deflection.

Table 1: Critical angle θ_c for different beam energies.

Energy [GeV]	$\boldsymbol{\theta_c}$ **[$\boldsymbol{\mu rad}$]**
120	18.3
270	12.2
400	10.0
450	9.4
6500	2.5
7000	2.4

2.1 TECA crystal specifications

The TECA crystal is installed in Long Straight Section 4 (LSS4) of the SPS and is employed for experimental studies on crystal-assisted slow extraction. Unlike the TECS crystal in LSS2, which locally shadows the electrostatic septum, TECA operates in a *non-local shadowing* configuration. Its role is to reduce the beam losses on the ZS septum downstream and it's also used for Machine Development (MD) purposes.

The crystal is a bent silicon strip with a length of a few millimetres and a bending angle of several hundred microradians, optimized for channelling 400 GeV/c protons. For such particles, the critical angle for channelling is about 10 μrad, requiring sub-microradian alignment precision. It is possible to observe the specifications of this crystal in Tab.2.

Table 2: Specifications of the TECA bent crystal.

Parameter	**TECA**
Number of crystals	2 (1 + 1 spare)
Crystal location	Upstream of VB.BB.41779 in LSS4
Crystal orientation	Actuated from INSIDE, deflecting in CH towards INSIDE
Crystal thickness	$\approx 1800\,\mu$m
Total CH deflection angle	$> 150\,\mu$rad (towards INSIDE)
Nominal crystal position	≈ -50.0 mm from axis (INSIDE side of SPS)
Nominal crystal angle	≈ -1.23 mrad w.r.t. nominal axis, towards INSIDE

2.2 Goniometer and holder

The TECA crystal in LSS4 is mounted on a high-precision goniometer developed at CERN for bent crystal experiments in beam collimation and extraction [17]. The system fulfills the stringent requirements of crystal channelling, where alignment tolerances are of the order of a few µrad.

The goniometer provides two rotational degrees of freedom: a fine angular adjustment around the vertical axis with a step resolution of approximately 1 µrad, enabling precise alignment of the crystal planes with respect to the circulating beam, and an orthogonal tilt axis with coarser resolution for systematic scans. In addition, the device allows linear translation of the crystal by several tens of millimetres inside the vacuum chamber (up to ~ 35 mm from the beam center), which permits insertion into and retraction from the beam halo.

The crystal holder is an ultra-high-vacuum compatible support that ensures mechanical stability at the sub-µrad level while minimizing vibrations and thermal drifts. The bent silicon strip is securely clamped, and fiducial markers are integrated to facilitate beam-based alignment as shown in Fig. 8. The system guarantees a reproducibility of repositioning within a few microns after retraction. The distance between the crystal and the holder is 34.5 mm.

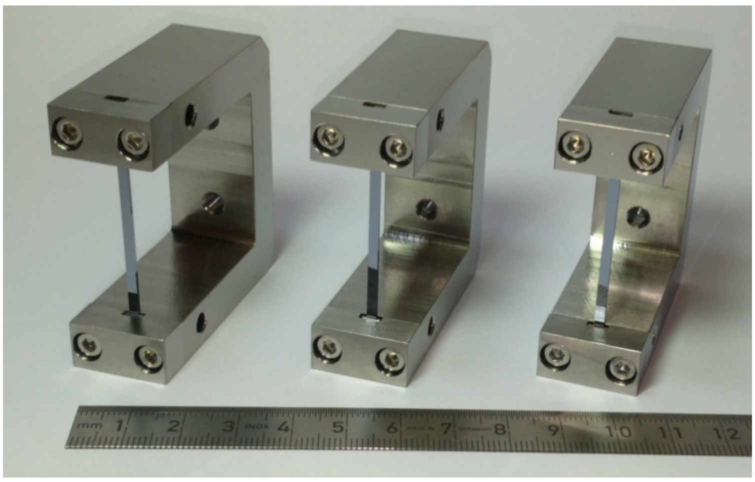

Figure 8: Crystal holder developed at CERN for bent crystal experiments [18].

2.2.1 Crystal position in beam referential

The TECA crystal is positioned in the inner side of the ring as explained in Tab.2 and displayed in Fig. 9.

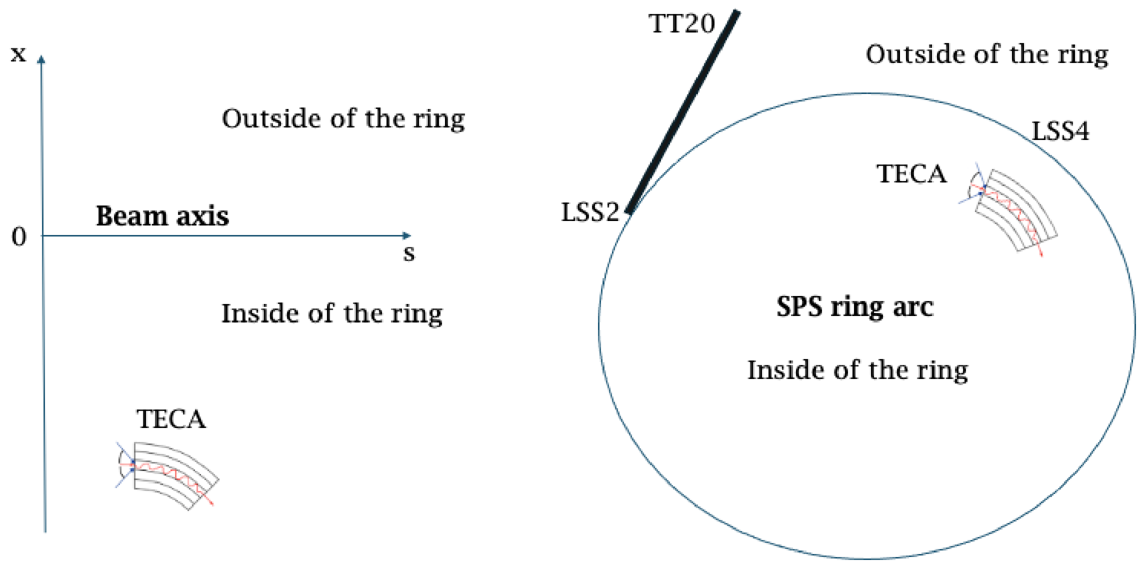

Figure 9: On the left side of the figure is shown the TECA position within respect to the beam axis, showing that the crystal has a negative horizontal position. On the right side of the figure, a schematic overview of the SPS ring showing that the crystal is inside the ring and that the extraction line in LSS2 is in the outside of the ring.

2.3 EverestCrystal in Xsuite simulation

The crystal in simulated through a model called EverestCrystal which has the following characteristics:

```
crystal = xc.EverestCrystal(
    length = 2e-3,
    material = xc.materials.SiliconCrystal,
    bending_angle = 88e-6,
    side = "left",
    lattice = "strip",
    jaw = 72e-3,
    tilt = 200e-6,
    width = 200e-3,
    height = 50e-3
)
```

where length is the longitudinal dimension, jaw the horizontal position , tilt the angle with the beam axis, width is the horizontal dimension and height is the vertical dimension of the crystal.

The use of pencil beams in the simulation provides a convenient way to probe the response of the crystal. Each pencil beam is defined by a fixed set of coordinates (x, p_x) and negligible spread, so that the interaction of particles with the crystal can be studied in a highly controlled manner. By scanning several pencil beams over different incident positions and angles, it is possible to map the channelling acceptance of the crystal and quantify how the efficiency varies across phase space. In particular, the Gaussian fit of the channelled particles (see Fig. 10) allows one to characterize the angular divergence of the channelled fraction with respect to the incident direction of the beam.

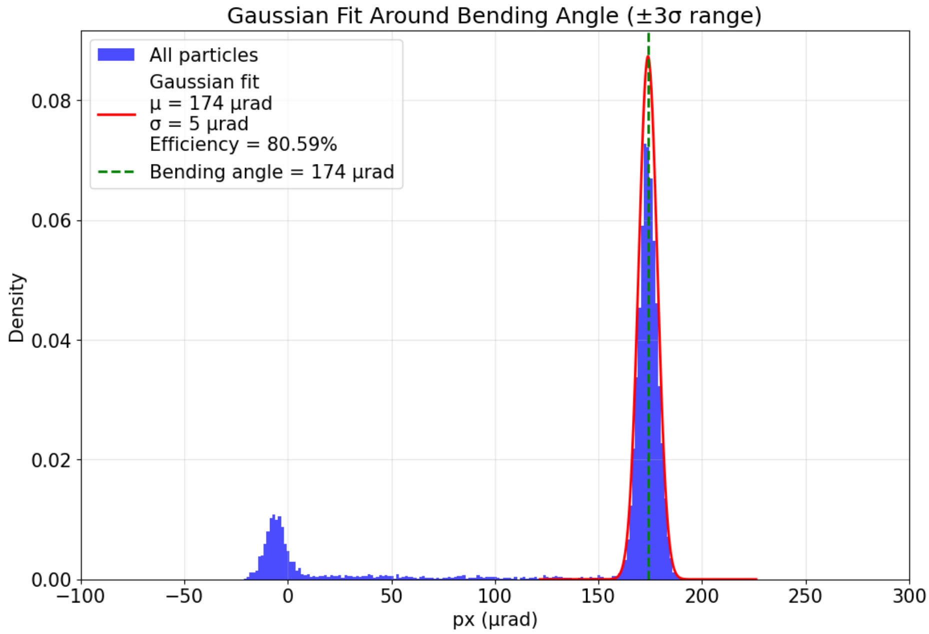

Figure 10: Gaussian fit of the channelled particles of a pencil beam passing through a crystal with the same features of TECA.

Outside the critical angle range, the channelling efficiency rapidly decreases to zero as it is possible to see in Fig. 11. For this reason it is crucial to properly align the beam with the crystal tilt.

These benchmarks with pencil beams form the basis for later integration into the full SPS extraction scheme. They establish the intrinsic response of the crystal before including the machine optics, bumps, and dispersion functions required to drive particles onto the crystal in a realistic accelerator cycle. In this way, the pencil beam studies serve as a reference to disentangle the pure crystal physics from the effects of the surrounding SPS lattice, ensuring that the measured extraction efficiencies in global simulations can be correctly interpreted.

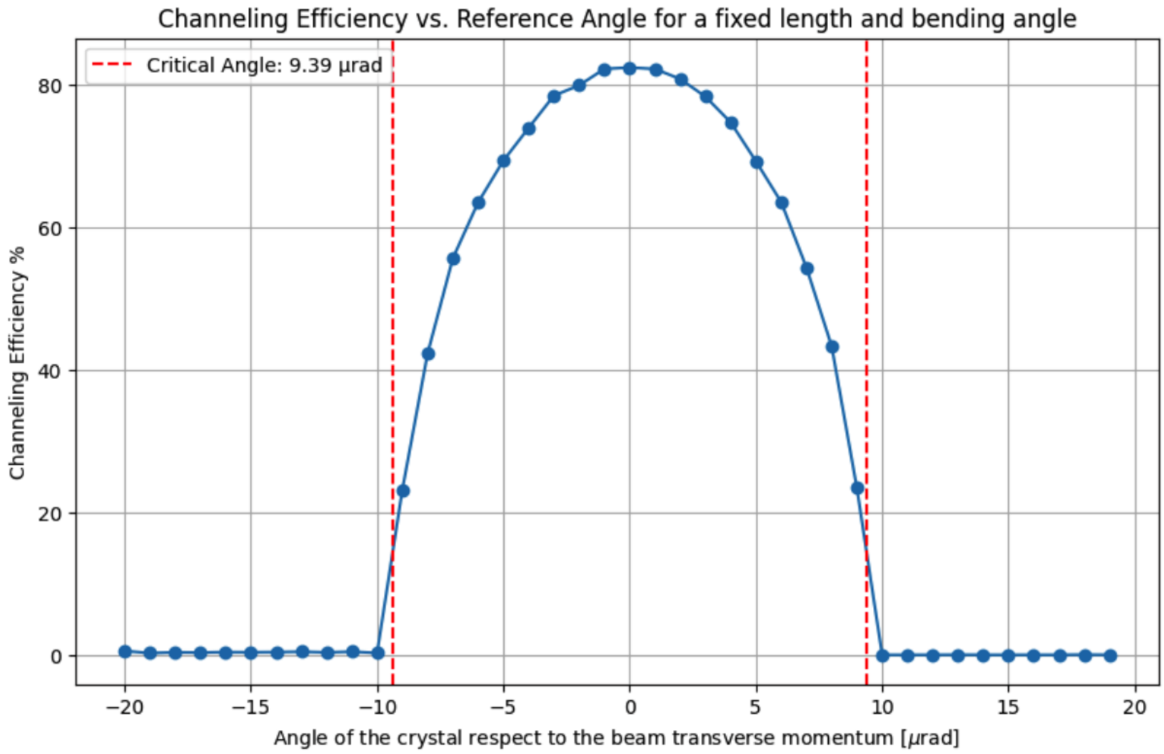

Figure 11: Channelling efficiency for different impacting angles of a pencil beam passing though a crystal with the same features as TECA.

3 Extraction concept modeling

In order to perform the non-resonant extraction, new optics were needed in order to have high dispersion for the reference-momentum-change steering. The first step was indeed to find the optics with the proper features for this scheme. To perform these optics studies the parameters in the Tab 3 were used.

Table 3: Beam parameters for the SPS slow extraction.

Parameter	**Unit**	**Value**
Particle	p	–
Momentum (p_0)	GeV/c	400
Relativistic factor ($\beta_r\gamma_r$)	–	426
Magnetic rigidity ($B\rho$)	Tm	1334
Momentum spread ($\Delta p/p_0$)	‰	[−1.5, 1.5]
Horizontal emittance (rms, norm.) ($\varepsilon_{x,n}$)	μm	10
Vertical emittance (rms, norm.) ($\varepsilon_{y,n}$)	μm	5

3.1 Optics studies

In order to achieve this dispersive driven extraction technique it is crucial to study possible optics with some specific requirements. This study has been done by using the Twiss tables of the different optics by scanning the tunes from 15 to 27 with an offset of 0.05 between the horizontal and the vertical ones. :

- High dispersion term over betatronic term at the crystal location (the ratio between the two term in Eq. 1)
- Aperture Δx_{col} bigger than TPST thickness (4.2mm).
- The dimensions of the beam (vertically and horizontally) must be reasonable (a threshold of 20 mm was set for the horizontal dimensions).

The separation Δx_{col} has been calculated both at the TPST (extraction point in LSS2) and at the TCSM (collimator in LSS4) in case it would have not been possible to directly extract in LSS2, it is possible to observe the sinusoidal trend of the separation at the two different collimators in Fig.12. Although several tunes fulfilled the criteria in Tab. 4, the dispersion at TECA and TPST followed the same sign, which prevented achieving the ideal opposite-sign configuration. This limitation required considering alternative strategies, such as placing the beam between the crystal and the chamber wall to recover the necessary separation at extraction. Nevertheless, the Q22 optics was selected as the most suitable solution, since it already exists in the SPS databases and provides sufficient dispersion to drive the beam into the crystal while respecting aperture constraints.

Table 4: Beam parameters at TECA, TPST and TCSM for different tunes.

Tune	16.1	19.1	22.1	25.1
σ_x^{MAX} [m]	0.02	0.02	0.01	0.01
β_x at TECA [m]	80.50	71.30	65.40	61.70
D_x at TECA [m]	4.64	−3.70	1.47	−2.19
μ_x at TPST [2π rad]	10.70	12.70	14.70	16.70
μ_x at TCSM [2π rad]	2.79	3.31	3.82	4.34
$\frac{D_x}{\beta_x}$ at TECA	0.06	−0.05	0.02	−0.04
Δx_{col} at TPST [mm]	12.80	11.20	10.00	9.30
Δx_{col} at TCSM [mm]	10.30	−8.30	6.80	−5.60

From the Tab. 4 it's possible to see that the optics were chosen in concomitance with the positive peaks of the sinusoidal function of the separation $\frac{D_x}{\beta_x}$ at TPST. These optics also have a separation at TCSM that is close to the peaks but in this case it is not necessary being on the positive side of the sinusoidal function, indeed in the parameters we can see that we have negative separations for two of the selected optics. In the end the selected optic was the **Q22** ($Q_x = 22.13$, $Q_y = 22.18$) and the reason is that this optic already existed in the databases while the other candidates were not.

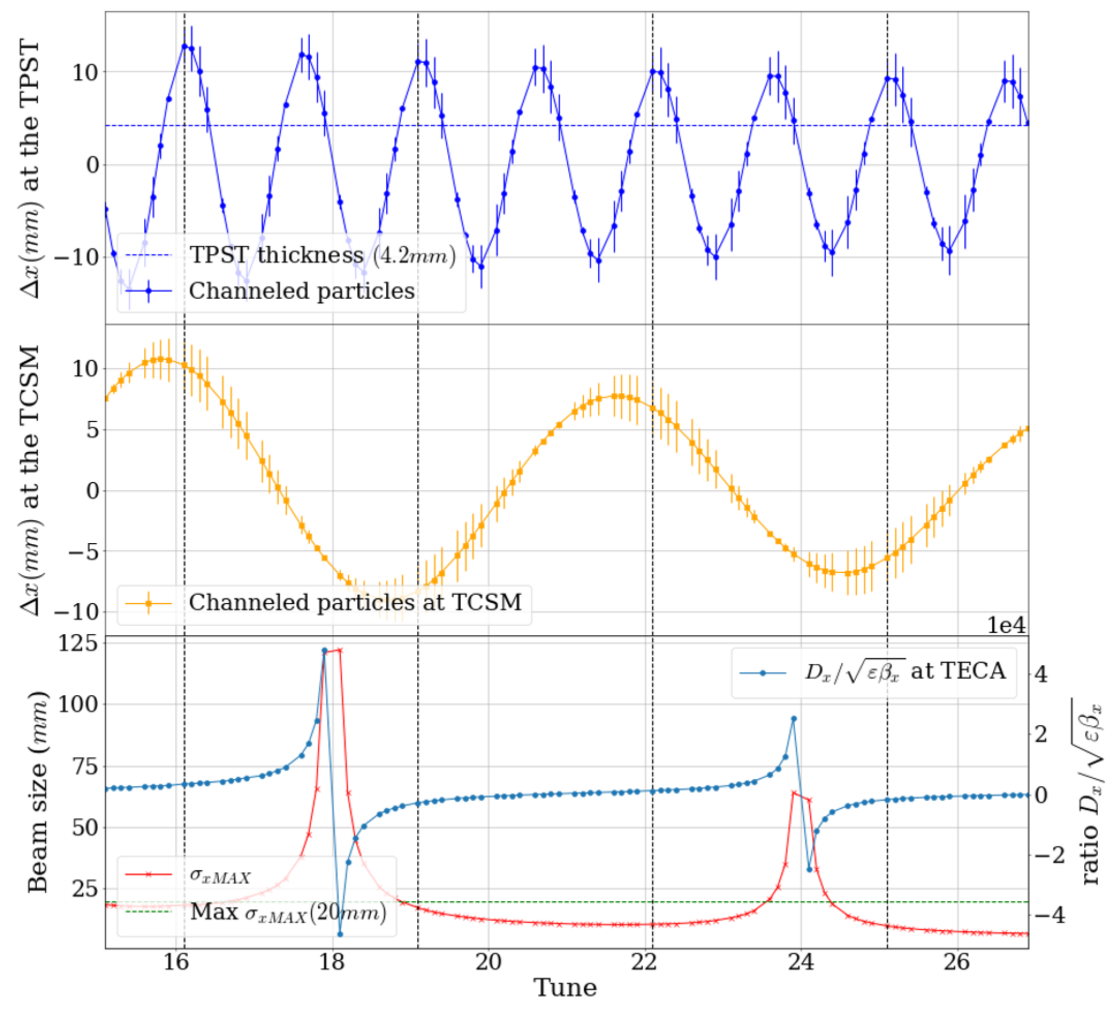

Figure 12: Optics scan from a tune equal to 15 to 27. The vertical dashed lines represent the best candidates.

3.1.1 Dispersion sign problem

Since the extraction in LSS2 takes place in outer side of the ring and the crystal is in the inner side of the ring, the ideal scenario would be with opposite dispersion sign at these two locations. The reason behind this is that ideally, in LSS4, the beam should come from the inner side of the ring with the bump on in order to touch the crystal from the side closer to the beam axis. The problem is that if the beam is pushed into the crystal from this side, the particles with low momentum will touch first the crystal in LSS4 and they would receive a kick from it, but these particles are the ones that are the most far away from extraction point in LSS2. This can be seen in the illustration in Fig. 13. Unluckily, as already mentioned in 3.1, the ratio dispersion/betatronic at TECA and at TPST follow the same exact trend so it is not possible to find optics in SPS that satisfy the requirement of having opposite dispersion terms.

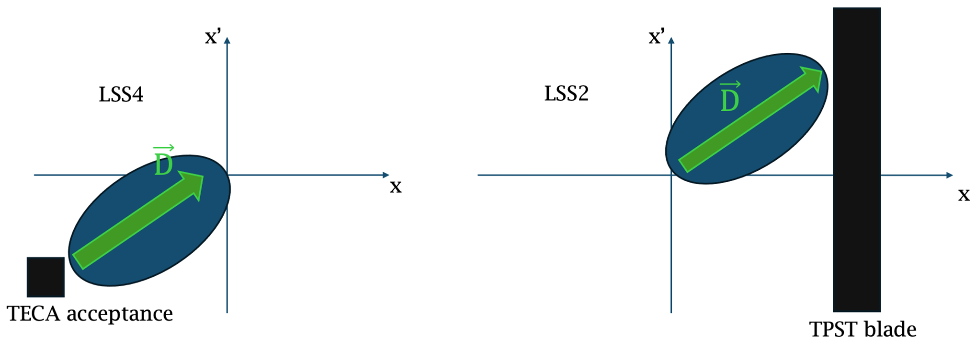

Figure 13: Phase space at TECA (left) and at the extraction septum (right). Because the dispersion has the same sign at both locations, the particles with lower momentum are displaced toward the crystal in LSS4, but these same particles are further away from the septum blade in LSS2. This mismatch prevents an ideal correlation between crystal deflection and extraction.

To better illustrate the adopted solution, Fig. 14 shows the phase space at TECA and at the extraction point. By steering the beam between the crystal and its mechanical holder, the first particles to interact with the crystal are those with higher momentum, which are also closer to the septum blade at LSS2.

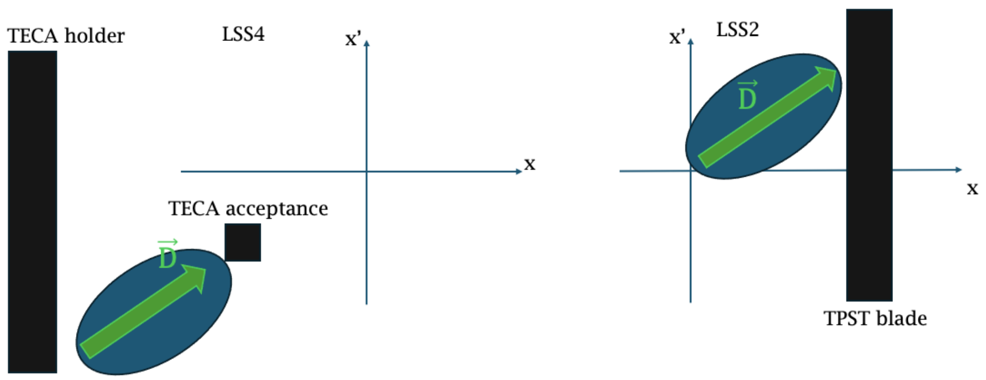

Figure 14: Phase space at TECA (LSS4, left) and at the extraction septum (LSS2, right). The beam is displaced between the crystal and its mechanical holder so that higher-momentum particles touch the crystal first.

By placing the beam between the crystal and its mechanical holder using a local orbit bump as shown in Fig. 15, the first particles to touch the crystal are those with higher momentum. These are naturally displaced closer to the extraction septum in LSS2, making them the best candidates for successful extraction despite the unfavorable dispersion condition.

Once the optics were selected, the sequence was set up with the correct tune and chromaticity. At this point, there's the need of a bump that brings the beam to the crystal in

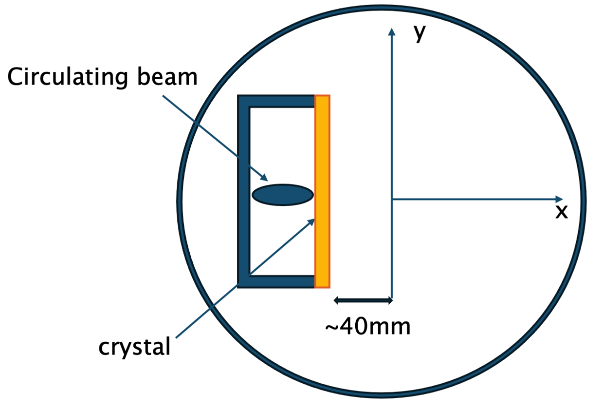

Figure 15: Sketch of the physical space at the TECA location.

order to start the channelling of the beam that leads the extraction.

3.2 LSS4 bump

The approach used to create a bump in LSS4 was to generate three different knobs: one for optimising the beam position and angle close to the crystal (K_0) and two fine orthogonal knobs that steer the beam either in position or in angle orthogonally (K_x for 1 mm and K_{px} for 1 μrad). The final strength of each corrector looks like this:

$$K_i = K_0 \cdot \alpha_i + K_x \cdot \beta_i + K_{px} \cdot \gamma_i \tag{3}$$

where α_i is the strength of the corrector for when K_0 is equal to 1 and the other to knobs are set to zero and similarly for the other two sets of values β_i and γ_i.

The introduction of orthogonal knobs is essential because the action of a single corrector generally modifies both the transverse position x and the angle p_x of the beam simultaneously. By constructing two additional knobs that act orthogonally in phase space, it becomes possible to steer the beam at TECA either purely in position or purely in angle. This decoupling is crucial for fine alignment with the crystal, since optimal channelling strongly depends on matching the beam trajectory to the crystal orientation.

In LSS4 there are four correctors that can be used to generate a bump strong enough to bring the beam to crystal. The strength of the respective correctors for each knob is illustrated in the Tab. 5.

Table 5: Knob decomposition in main knob, orthogonal position (1 mm) and orthogonal angle (1 µrad).

	MPSH.41402	MPLH.41658	MPLH.41994	MPSH.42198
Main knob	-3.08×10^{-4}	-4.93×10^{-4}	-5.04×10^{-4}	-9.62×10^{-5}
Orthogonal pos (1 mm)	2.26×10^{-5}	-2.70×10^{-6}	2.18×10^{-5}	-1.65×10^{-5}
Orthogonal angle (1 µrad)	-6.73×10^{-7}	6.75×10^{-7}	-4.11×10^{-7}	8.53×10^{-7}

Furthermore, the four correctors in LSS4 are combined in such a way that they generate a local orbit bump, which closes outside of the insertion region. In this configuration, the orbit distortion is confined to LSS4 and the global optics of the SPS ring remain unaffected. This ensures that the beam can be brought into the crystal acceptance without introducing undesired orbit perturbations in the rest of the machine.

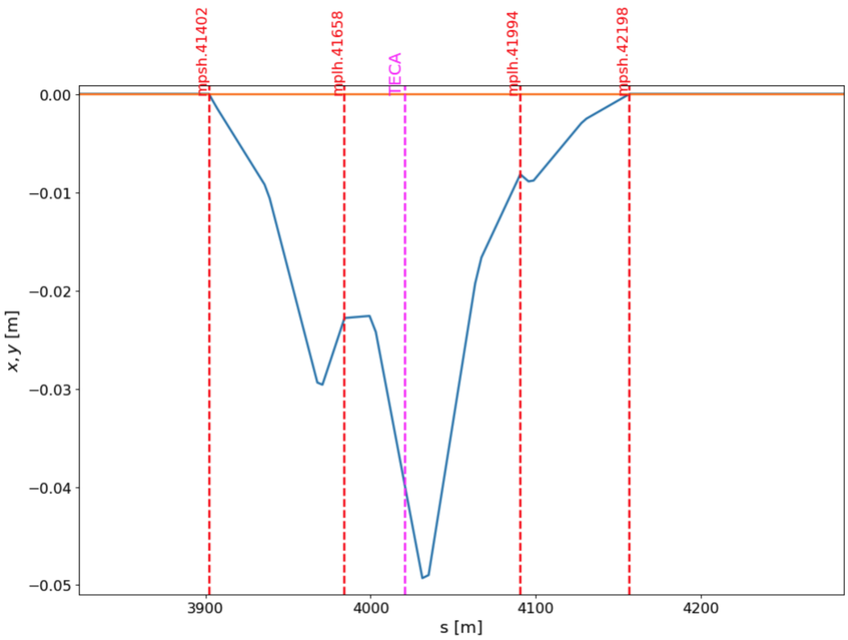

Figure 16: Bump shape in LSS4.

It is possible to see the shape of the bump when K_0 is set to 1 in Fig. 16. When K_0 is set at 1 the coordinates at TECA are (x, p_x) = (- 40 mm, - 0.8884 mrad).

All these studies were saved in a dedicated repository [19].

3.3 Extraction simulation

The simulation has been set up with the following characteristics:

- ZS retracted
- Normalized horizontal emittance: 4 µm rad
- Normalized vertical emittance: 5 µm rad
- $\delta p/p_0 = 1.5 \times 10^{-3}$
- The energy ramp to move the beam on the dispersion vector: ±0.8 GeV

3.3.1 Plan A: extraction in LSS2

As it is possible to see in Fig. 17, the extraction is slow since the particles get extracted all over the number of turns. Moreover in Fig. 18 it's possible to see that the particles properly reach the crystal since the distribution of the number of interactions with the crystal follows a geometric distribution with a p of 0.8 which is the channelling efficiency estimated in Sec. 2.

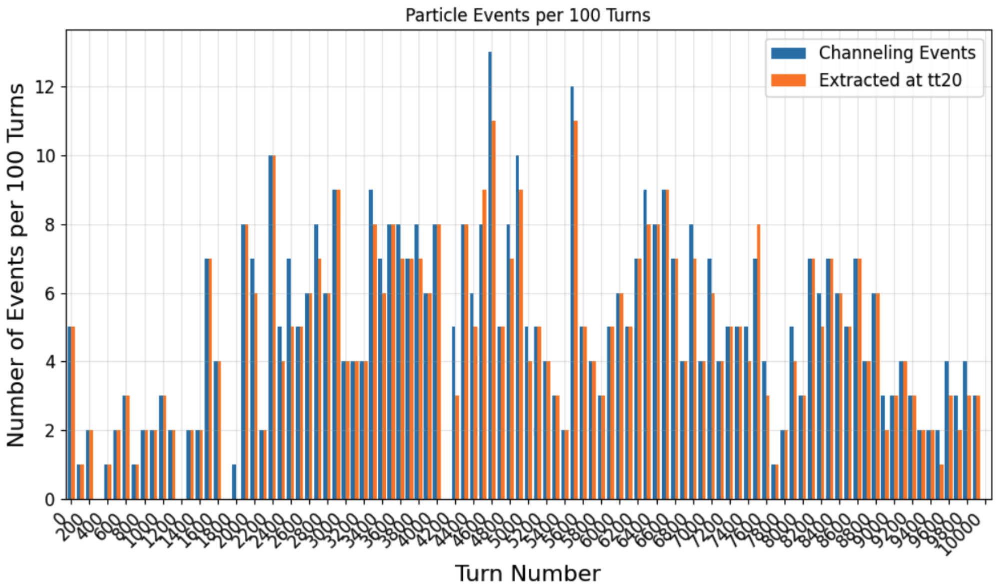

Figure 17: Time evolution of the extraction, showing how the particles get extracted throughout the entire simulation.

The phase spaces of the beam at TECA in Fig. 19 and at TPST in Fig. 20 show how the particles reach the crystal at its acceptance and consequently how the channelled particles jump over the collimator blade thanks to the kick received by the crystal. In the two figures it is possible to see the different momentums: the color scale indicates that if the particles is represented with a lighter green it has higher energy. The particles with higher energy touch the crystal before than the particles with low energy and get extracted first. While the energy ramps down, the particles drift closer to the center at TECA and get channelled

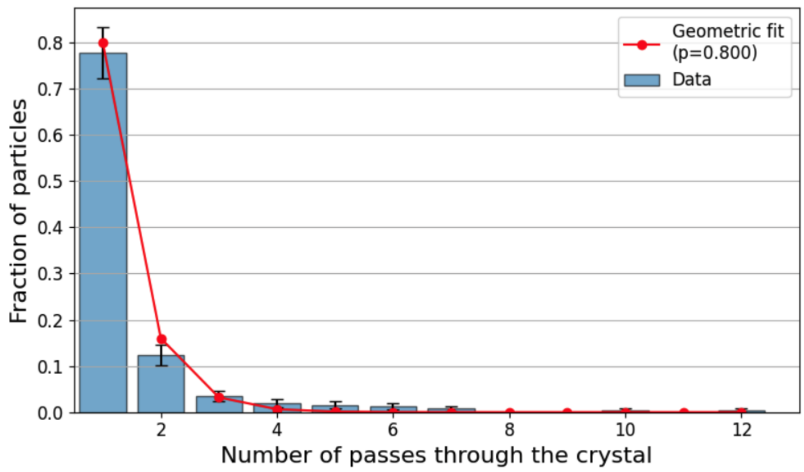

Figure 18: Geometric distribution of number of passes through the crystal with a p = 80 %

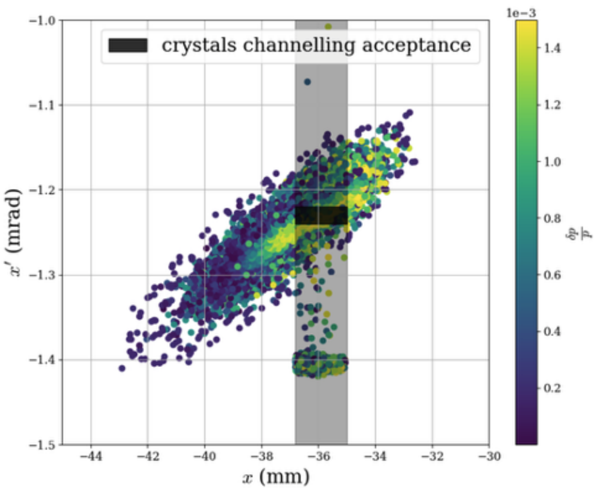

Figure 19: TECA phase space.

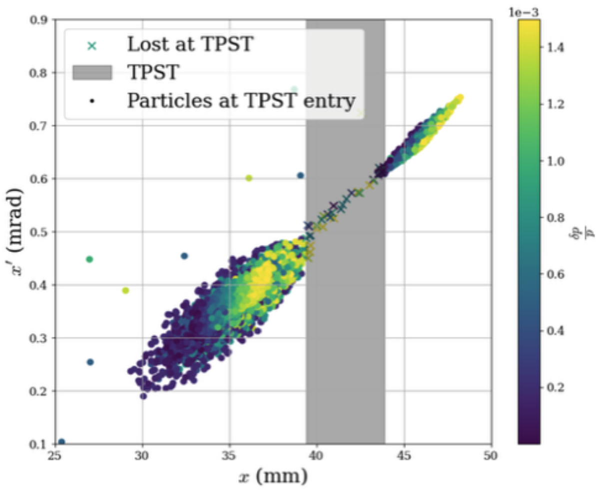

Figure 20: TPST phase space.

while at TPST the particles drift outward and consequently the particles that received the kick from the crystal get extracted.

In the end the achieved extraction efficiency, computed as if the particles reach the end of the extraction line in TT20, is 95 % while 3 % of the particles hit the TPST collimator and the rest is lost on the crystal.

3.3.2 Plan B: TCSM collimation

In case it was not possible to place the beam between the crystal and its holder, the back-up plan was using the TCSM collimator to see if the particles were properly channelled by the crystal. In Fig. 21 it is possible to see the channelled particles on the right side of the plot while the core is on the beam axis at $x = 0$. The collimator would scrape in and block the channelled particles.

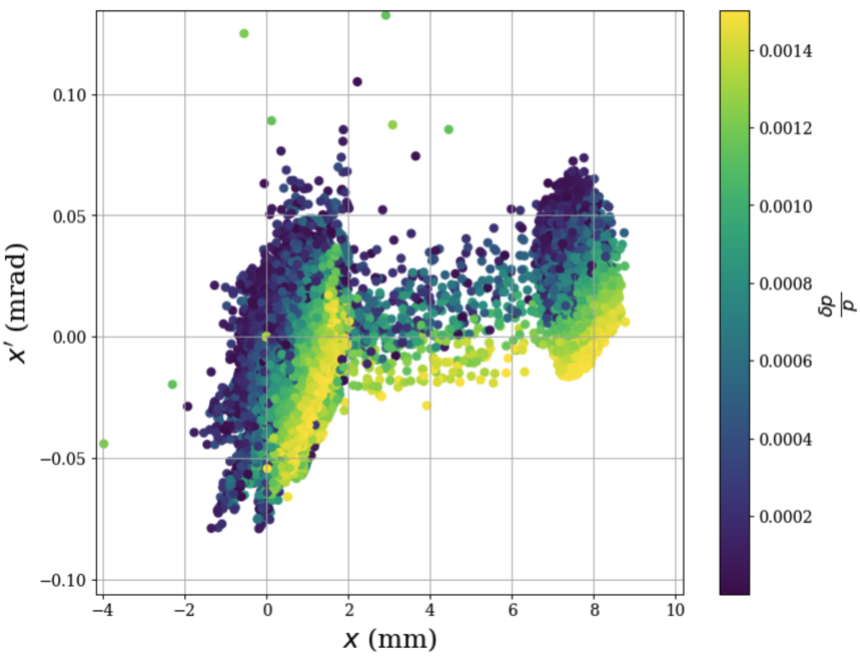

Figure 21: TCSM phase space showing the circulating beam on the left, the de-channelled particles in the middle and the channelled particles on the right.

4 Machine Development (MD)

4.1 MD plans

Two parallel and a dedicated Machine Development (MD) have been done. The plan has been divided in two. The first part consisted in creating the bump in LSS4 and see its stability. Once the knobs have been inserted in LSA application, the next step is the injection at 14 GeV; at this stage the bump has been increased until a max amplitude. The goal was to see until what amplitude the beam wouldn't be lost, after this threshold the system would trigger an interlock and dump the beam. Probably the beam would hit an element downstream the crystal. After seeing the stability of the beam at this stage, the next step would be to ramp the energy from 14 GeV to 400 GeV.

Once these preliminary studies would be done, the next steps would be carried out during the dedicated MD. The first step is to retract the ZS and the TECA and lower the bound of the interlock for the ZS Beam Loss Monitors (BLMs). Then turning on the bump again and create the two different energy ramps for both Plan A and Plan B. Once one of the two Plan seems to be more reliable, the next step is to align the TCSM and the crystal.

4.2 MD results

These early tests were carried out with the TECA crystal in the retracted position. In order to generate and control the bump, three dedicated knobs were defined and implemented in LSA, as reported in Tab. 5. The so-called *main knob* was gradually increased until the system reached the interlock threshold, thereby defining the operational range of the bump amplitude. At the beginning of the study, the beam was injected at an energy of 14 GeV without an energy ramp. This allowed us to verify the stability of the orbit at flat-bottom and ensure that no unforeseen instabilities or losses were present. Once a sufficiently stable configuration was achieved, the energy ramp was enabled.

It became evident from the first two plots of Fig. 22 that during the ramping process, the closed orbit in LSS4 exhibited a noticeable drift with respect to its reference trajectory. This effect pointed to a mismatch between the optics settings at flat-bottom and their evolution during the ramp. Since the local bump stability is crucial for steering particles onto the crystal, it was necessary to investigate the use of orbit correctors to counteract this drift and maintain the desired orbit throughout the energy cycle.

To quantify and mitigate the observed deviation, we relied on the formalism of linear optics. The transverse displacement induced at a given location s (in our case, the BPM BPCE.41801, located just downstream TECA) by a set of correctors providing kicks θ_i can be expressed as

$$\Delta x(s) = \frac{\sqrt{\beta(s)}}{2\sin(\pi\nu)} \sum_{i=0}^{N} \theta_i \sqrt{\beta(s_i)} \cos(|\phi(s) - \phi(s_i)| - \pi\nu) , \tag{4}$$

where $\beta(s)$ and $\phi(s)$ denote the optical beta function and phase advance at location s, while ν is the horizontal betatron tune. This relation allowed us to identify the optimal set of correctors to counteract the ramp-induced drift and stabilize the orbit near the crystal location.

In order to minimize the orbit distortion observed at the BPM closest to the TECA crystal (BPCE.41801), a numerical procedure was implemented to determine the most effective location and strength of a hypothetical corrector.

To quantify the quality of the correction, a loss function is defined as the root mean square (RMS) value of the residual orbit, after adding the effect of the trial corrector:

```
loss = lambda x: np.sqrt(np.mean((orb + dx(kick=x[0], s=x[1]))**2))
```

where $x[0]$ corresponds to the kick strength and $x[1]$ to the candidate longitudinal position of the corrector.

The minimization of this function is carried out using the `differential_evolution` algorithm from the SciPy library, which explores the parameter space globally:

```
result = differential_evolution(loss,
           bounds=[(-1, 1), (0, twiss['s'].max())])
```

The output of the optimization provides the optimal corrector parameters $[\theta, s_c]$ that minimize the orbit RMS at the BPM of interest, effectively identifying the best location in the lattice to compensate for the observed drift. A set of correctors was then found, they are shown in the Tab. 6:

During the cycle, the orbit movement was flattened to an RMS variation of about ±5 mm as it is possible to see in Fig. 23 by applying corrections with a set of horizontal correctors chosen from the list in Tab. 6, mainly at flat top with kicks in the range of 20–25 µrad.

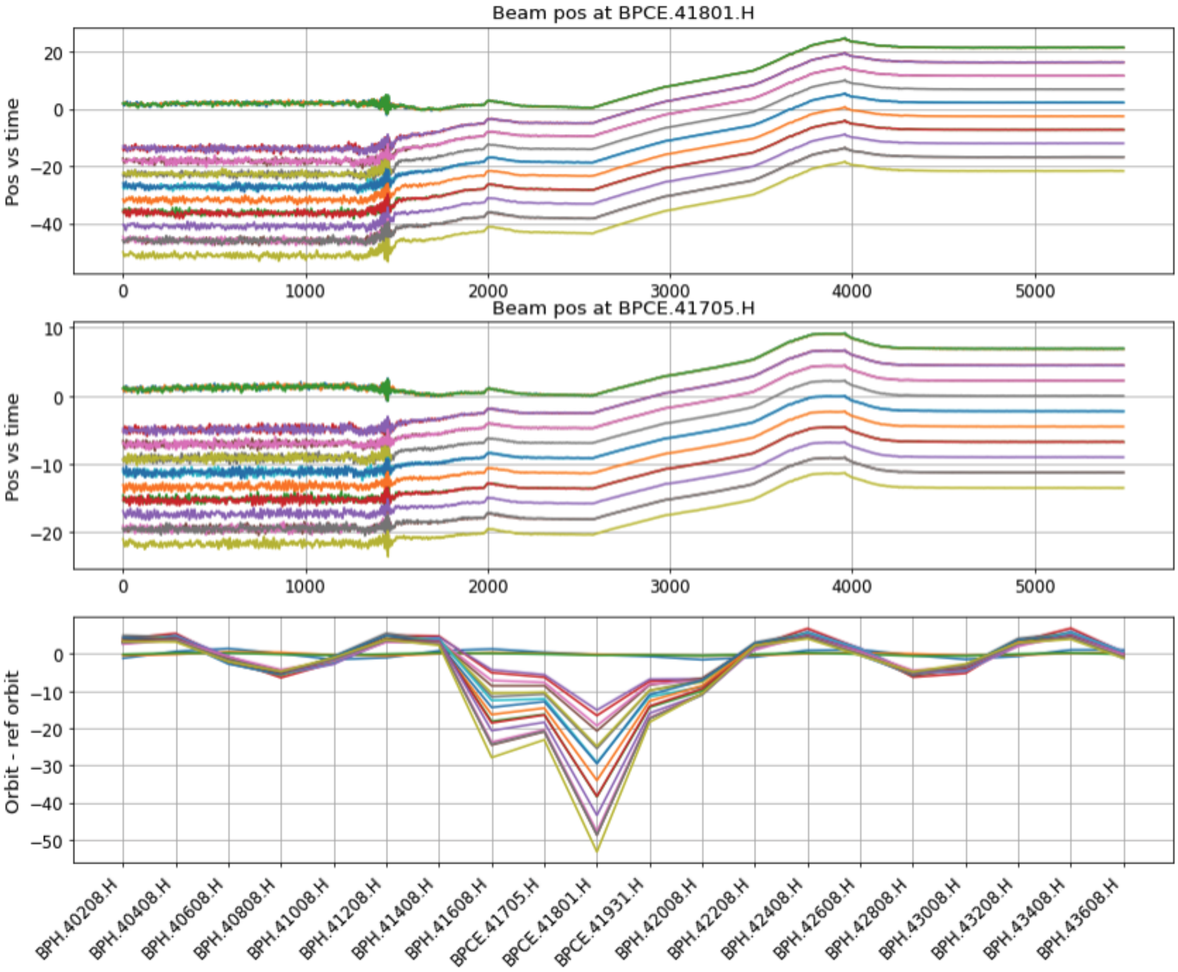

Figure 22: BPMs scan of the orbit in LSS4 throughout the ramp. The first two plots show the time-dependency of the orbit at the two closest BPMs to TECA. The bottom plot shows the orbit at 500 ms from injection.

Table 6: List of correctors and their correction sign.

Corrector	Correction sign
MDH.20207	Negative
MDH.31007	Positive
MDH.40807	Negative
MDH.42807	Negative
MDH.52607	Positive
MDH.53607	Positive
MDH.63407	Negative

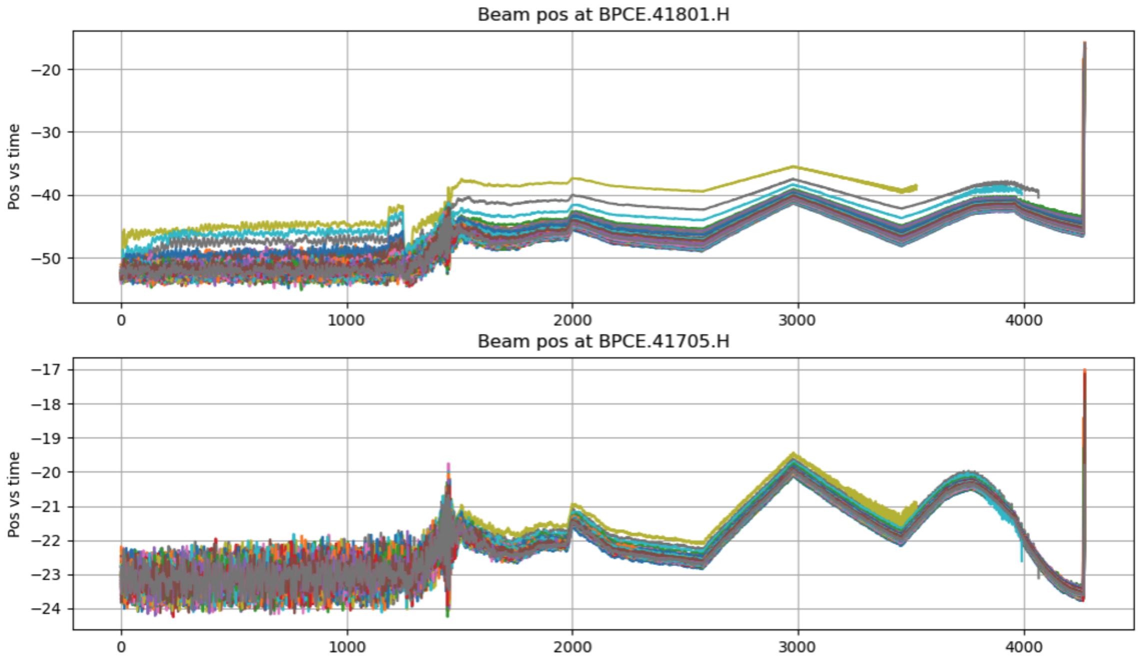

Figure 23: Scan after flattening the orbit with the correctors.

During the dedicated MD for the non-resonant extraction with the TECA crystal was carried out with the ZS retracted and with the BLM interlock limits in LSS2 lowered. The momentum ramping at flat-top was configured either from 400 GeV to 400.4 GeV or from 400 GeV to 399.6 GeV. This choice was done so that we could shift to the back-up plan in case something would have gone wrong. A scan of the TCSM jaws was performed, as visible in the Fig.24 to localize the beam core under these conditions. The onset of BLM signals indicated that the beam touched the jaws at 8.5 mm (left, outer) and −12.5 mm (right, inner).

The first attempt consisted of injecting the beam into the gap of the crystal holder. The beam was cut, and the crystal was fully inserted at its maximum stroke position (39 mm at the goniometer, corresponding to −39 mm relative to the machine center). A subsequent scan in steps of 1 mm towards the inside of the ring revealed that the beam was located too far from the crystal. Consequently, the bump was increased to 1.12, which was the maximum achievable value before the beam started impacting the vacuum valve downstream of TECA,

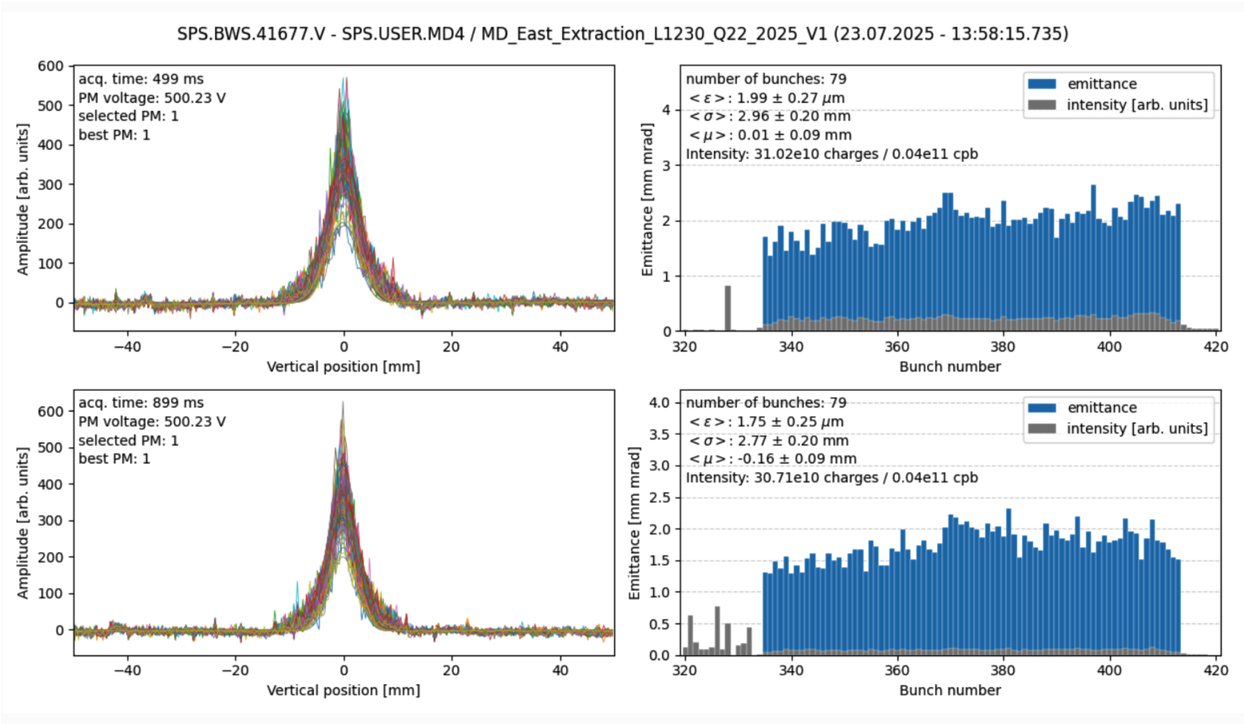

Figure 24: TCSM jaw scan.

triggering the BLM interlock. Under these conditions, BTC observed a surviving circulating fraction of only 20–30% of the initial beam intensity. The limited aperture between the crystal and downstream elements constrained the available phase space, and the strategy was revised to push the beam towards TECA from the machine center.

Xsuite simulations predicted an 8 mm separation between the channeled protons and the circulating beam. Based on this, the right TCSM jaw was selected as the absorber, expecting the channeled protons to intercept it within approximately five turns. A one-turn scheme was excluded due to the unfavorable dispersion direction at the collimator and the relatively large beam envelope of about ±10 mm, as confirmed by the TCSM jaw scan.

The crystal position was then scanned to identify the alignment working point. A noticeable rise in the BLM signal near TECA was observed at a stroke of 36.0 mm (−42 mm with respect to the machine center). However, the alignment procedure could not be completed due to lack of MD time.

At the end of the session, both TCSM and TECA were retracted, the ZS septum was reinserted, and the BLM thresholds in LSS2 were restored to their nominal values.

5 Conclusion

The studies presented in this work demonstrate that crystal-assisted non-resonant slow extraction is a promising candidate to mitigate the limitations of the conventional third-integer resonance scheme. Simulations performed with Xsuite show that extraction efficiencies above 95% are achievable when the ZS is removed from the line and the TECA crystal in LSS4 provides the initial deflection. Losses are largely reduced on the electrostatic septum, which is the dominant activation source in the present scheme, while only a few percent of the beam are lost on the crystal itself or on the TPST collimator. These results suggest that crystal-assisted extraction could significantly lower the long-term activation of LSS2 and enhance the sustainability of SPS operations.

However, the achieved efficiencies are still below the $> 99\%$ typically required for operational use. Further optimization of the crystal orientation, position, and goniometer alignment is expected to close this gap. Alternative optics configurations and novel solutions such as Multi-Volume Reflection Arrays (MVRA) are also being considered to increase the angle acceptance of the crystal and to improve extraction uniformity. Machine Development studies already showed that the local orbit bump in LSS4 can be generated and stabilized throughout the energy ramp, although residual orbit drifts must be corrected with additional correctors to preserve alignment stability.

The next step will be to validate these simulations experimentally in the SPS, with dedicated MDs foreseen to test the alignment procedures, measure the time structure of the extracted spill, and benchmark the predicted efficiencies. If successful, crystal-assisted non-resonant extraction could provide a cleaner and more robust alternative to the standard resonant scheme, reducing activation risks while maintaining high extraction quality. In the longer term, this concept may open the way for operational implementation of crystal septa in high-intensity accelerators, contributing to safer and more efficient delivery of beams to fixed-target experiments.

References

[1] K. Elsener et al. "Proton extraction from the CERN SPS using bent silicon crystals". In: *Nuclear Instruments and Methods in Physics Research Section B: Beam Interactions with Materials and Atoms* 119.1 (1996), pp. 215–230. ISSN: 0168-583X. DOI: https://doi.org/10.1016/0168-583X(96)00239-X. URL: https://www.sciencedirect.com/science/article/pii/0168583X9600239X.

[2] C. Ahdida et al. "The experimental facility for the Search for Hidden Particles at the CERN SPS". In: *JINST* 14.03 (2019). 21 pages, P03025. DOI: 10.1088/1748-0221/14/03/P03025. arXiv: 1810.06880. URL: https://cds.cern.ch/record/2644153.

[3] Bruno Balhan et al. "Improvements to the SPS Slow Extraction for High Intensity Operation". In: (2019). URL: https://cds.cern.ch/record/2668989.

[4] Matthew Alexander Fraser et al. "Demonstration of slow extraction loss reduction with the application of octupoles at the CERN Super Proton Synchrotron". In: *Phys. Rev. Accel. Beams* 22 (12 Dec. 2019), p. 123501. DOI: 10.1103/PhysRevAccelBeams.22.123501. URL: https://link.aps.org/doi/10.1103/PhysRevAccelBeams.22.123501.

[5] Francesco Maria Velotti et al. "Demonstration of non-local crystal shadowing at the CERN SPS". In: *Proceedings of the 14th International Particle Accelerator Conference (IPAC'23), Venice, Italy*. JACoW IPAC2023. 2023.

[6] Francesco Maria Velotti et al. "Septum shadowing by means of a bent crystal to reduce slow extraction beam loss". In: *Physical Review Accelerators and Beams* 22.9 (2019), p. 093502. DOI: 10.1103/PhysRevAccelBeams.22.093502.

[7] Matthew Fraser et al. "SPS slow extraction losses and activation: update on recent improvements". In: (2019), WEPMP031. DOI: 10.18429/JACoW-IPAC2019-WEPMP031. URL: https://cds.cern.ch/record/2693913.

[8] Matthew Alexander Fraser et al. "SPS slow extraction losses and activation: challenges and possibilities for improvement". In: *Proc. IPAC'17* (2017), pp. 611–614.

[9] V. Kain et al. "Resonant slow extraction with constant optics for improved separatrix control at the extraction septum". In: *Phys. Rev. Accel. Beams* 22 (10 Oct. 2019), p. 101001. DOI: 10.1103/PhysRevAccelBeams.22.101001. URL: https://link.aps.org/doi/10.1103/PhysRevAccelBeams.22.101001.

[10] Matthew Alexander Fraser et al. "Demonstration of slow extraction loss reduction with the application of octupoles at the CERN Super Proton Synchrotron". In: *Physical Review Accelerators and Beams* 22.12 (2019), p. 123501. DOI: 10.1103/PhysRevAccelBeams.22.123501.

[11] Stuart Turner. "CAS CERN Accelerator School 5th General Accelerator Physics Course". In: *Course held in Jyvaeskylae* (1994), pp. 7–18.

[12] G. Iadarola et al. "Xsuite: An Integrated Beam Physics Simulation Framework". In: *Proceedings of the 13th International Conference on High Intensity and High Brightness Hadron Beams (HB'23), Geneva, Switzerland*. 2024. DOI: 10.18429/JACoW-HB2023-TUA2I1.

[13] P. Arrutia. *Non-resonant momentum-driven slow-extraction*. Tech. rep. SLAWG 73. CERN, 2023. URL: https://indico.cern.ch/event/1334617/.

[14] V Kain et al. "Resonant slow extraction with constant optics for improved separatrix control at the extraction septum". In: *Physical Review Accelerators and Beams* 22.10 (2019), p. 101001.

[15] A.A. Asseev et al. "Peculiarities of using the bent crystal for the extraction of protons from the IHEP accelerator to the PROZA setup". In: *Nuclear Instruments and Methods in Physics Research Section A: Accelerators, Spectrometers, Detectors and Associated Equipment* 330.1 (1993), pp. 39–43. ISSN: 0168-9002. DOI: https://doi.org/10.1016/0168-9002(93)91302-4. URL: https://www.sciencedirect.com/science/article/pii/0168900293913024.

[16] V.M. Biryukov et al. "Crystal collimation as an option for the large hadron colliders". In: *Nuclear Instruments and Methods in Physics Research Section B: Beam Interactions with Materials and Atoms* 234.1 (2005). Relativistic Channeling and Related Coherent Phenomena in Strong Fields, pp. 23–30. ISSN: 0168-583X. DOI: https://doi.org/10.1016/j.nimb.2005.03.003. URL: https://www.sciencedirect.com/science/article/pii/S0168583X05002284.

[17] Q Demassieux et al. "Development of bent crystal manipulation systems for beam collimation and extraction at CERN". In: *JACoW IPAC* 2023 (2023), MOPA085. DOI: 10.18429/JACoW-IPAC2023-MOPA085. URL: https://cds.cern.ch/record/2886016.

[18] Luigi Salvatore Esposito et al. "Crystal for slow extraction loss-reduction of the SPS electrostatic septum". In: *Proceedings of the 10th International Particle Accelerator Conference (IPAC'19), Melbourne, Australia*. 2019, pp. 19–24.

[19] M.P. Giacomell. *Slow Extraction with Crystals gitLab repository*. https://gitlab.cern.ch/abt-optics-and-code-repository/projects/slow-non-resonant-extraction-with-crystal-sps.